DMD diffraction measurements to support design of projectors for test and evaluation of multispectral and hyperspectral imaging sensors

Joseph P. Rice[*a], Jorge E. Neira[a], Michael Kehoe,[b] and Rand Swanson[b]

[a]National Institute of Standards and Technology, Gaithersburg, MD, USA 20899
[b]Resonon, Inc., Bozeman, MT, USA 59715

ABSTRACT

We describe our use of Digital Micromirror Devices (DMDs) for the performance testing, characterization, calibration, and system-level data product validation of multispectral and hyperspectral imaging sensors. We have developed a visible Hyperspectral Image Projector (HIP), which is capable of projecting any combination of many different arbitrarily programmable basis spectra into each image pixel at up to video frame rates. For the full HIP, we use a scheme whereby one DMD array is used in a spectrally programmable source, to produce light having the spectra of materials in the scene (i.e. grass, ocean, target, etc), and a second DMD, optically in series with the first, reflects any combination of these programmable spectra into the pixels of a 1024 x 768 element spatial image, thereby producing temporally-integrated 2D images having spectrally-mixed pixels. The HIP goes beyond conventional Digital Light Processing (DLP) projectors in that each spatial pixel can have an arbitrary spectrum, not just an arbitrary color. As such, the resulting spectral and spatial content of the projected image can simulate realistic scenes that a sensor system must acquire during its use, and can be calibrated using NIST reference instruments. Here we discuss our current HIP developments that span the visible/infrared spectral range of 380 nm through 5400 nm, with particular emphasis on DMD diffraction efficiency measurements in the infrared part of this range.

Keywords: calibration, diffraction, digital micromirror device, DMD, imaging, hyperspectral, multispectral, projector, remote sensing, spectroscopy, test and evaluation, validation, video

1. INTRODUCTION

Current procedures for typical hyperspectral and multispectral imager test and evaluation involve presenting relatively simple scenes and spectra to the instruments under test (IUT). To enable the ability to test spectral imaging performance with more realistic and complex scenes that can appropriately test the IUT and its data retrieval algorithms at their limits, we are developing a Hyperspectral Image Projector (HIP). We have described various details of the HIP concept and applications previously.[1-8] As a brief overview of the concept, refer to Fig. 1. An input image cube (one frame of an image cube time sequence, for example) is first broken down into its component spectra and corresponding abundance images. The HIP spectral engine is basically a programmable spectrum generator. It rapidly generates light having the component spectra, one spectrum at a time, by displaying the binary spectral image on DMD1 that provides the spectrum. It is analogous to the color filter in a conventional single-chip Digital Light Processing (DLP[®]) projector, except that it can provide any number of arbitrarily programmable spectra on demand. While the HIP spectral engine provides a given component spectrum, the HIP spatial engine displays, on DMD2, the abundance image corresponding to that spectrum. The grey scale value of each pixel in the two-dimensional abundance image indicates the relative proportion of the corresponding component spectrum required by the image cube. Upon projection of the entire set of component spectra and corresponding abundance images in sync with each other during the integration time of the IUT (or reference instrument, used for calibration of the projected image), the IUT (or reference instrument) will have measured the entire data cube for that frame. This mode of operation is exactly analogous to the rapid serial projection of red-green-blue spectra to simulate color images common in DLP and other video technologies. However, the HIP is

[*]Correspondence: joe.rice@nist.gov

not limited to arbitrary color – it can provide arbitrary spectra. Also, it is not limited to the visible spectral range. Both of these advances over conventional DLP technology are significant for applications to hyperspectral and multispectral imagers, as these instruments are capable of resolving spectra at high resolution over wide spectral ranges, including the ultraviolet and the infrared.
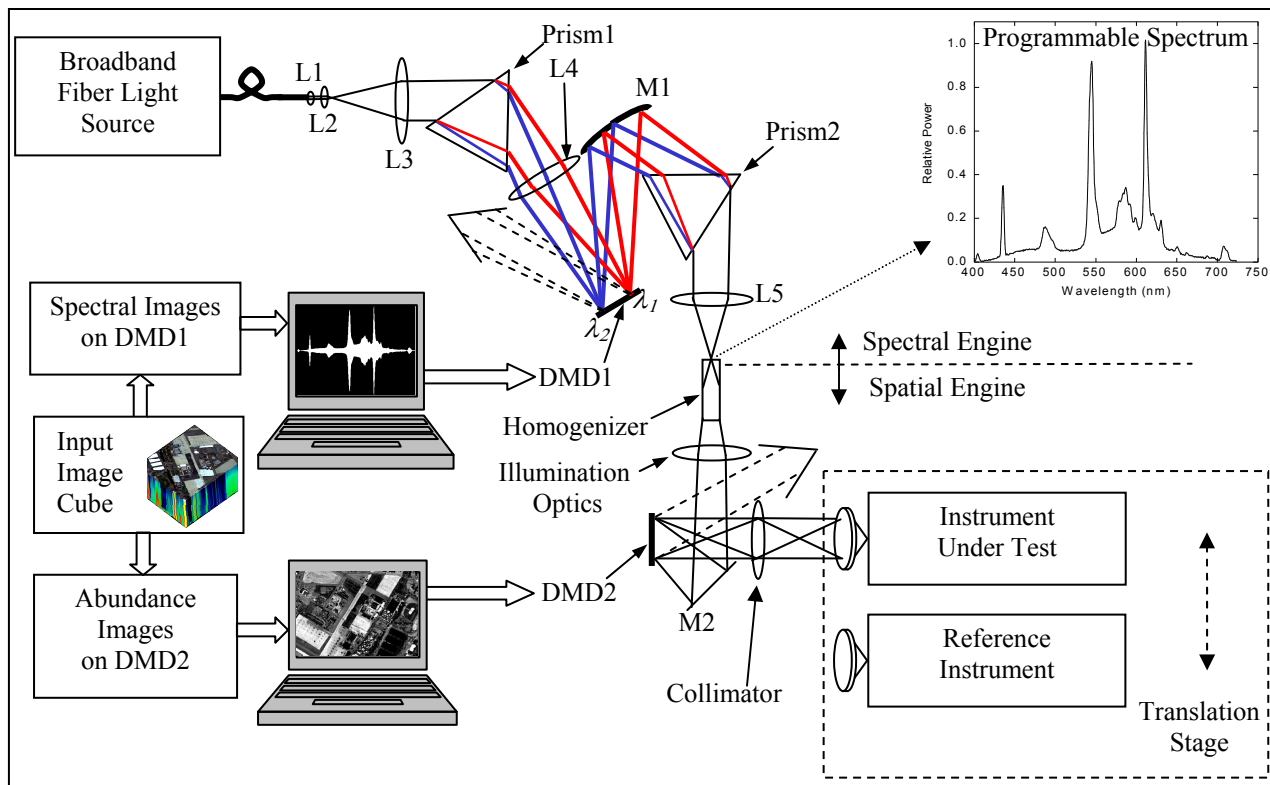

Figure 1. Concept of the Hyperspectral Image Projector (HIP). L=lens. M=mirror.

We are currently developing a prototype of the HIP operating in the visible--near-infrared (VNIR), short-wavelength infrared (SWIR), and mid-wavelength infrared (MWIR) spectral ranges. Our targeted ranges correspond roughly to the conventional usage for these terms: VNIR: 380 nm to 1100 nm; SWIR: 1000 nm to 2500 nm; MWIR: 3000 nm to 5400 nm. The DMD micromirrors are coated with aluminum, which has high reflectivity over these spectral ranges. However, since the infrared wavelengths approach the size of the micromirrors and the micromirror pitch of the available DMDs, diffraction by the DMD must be considered in the optical design of the HIP. This is true for both the spectral engine DMD1, which operates with normal incidence and oblique reflection (Fig. 1), and the spatial engine DMD2, which operates with oblique incidence and normal reflectance (Fig. 1). Thus, in this paper we discuss the diffraction efficiency of the DMDs that we plan to use in the HIP. We first describe a simplified diffraction model of the DMD that is useful for spectral engine design purposes, and then we report on diffraction efficiency measurements in the SWIR and in the MWIR in the sections that follow.

2. DMD DIFFRACTION MODEL

The DMD can modeled as a double-ruled diffraction grating, where one axis of the grating is rotated 90 degrees about the DMD normal from the other, thereby providing a two-dimensional array of diffraction spots.[9] The effect on grating efficiency of having all of the DMD micromirrors in the on (or the off) state can be modeled by regarding the DMD as a one-dimensional blazed diffraction grating[10] as depicted in Fig. 2. The lines of this grating are parallel to the micromirror hinges, which are at 45° to the DMD edges for the types of DMDs considered here. In this model, the micromirrors act as blazed facets of the grating, at angle ϕ to the DMD normal. The angle ϕ is simply the tilt angle of the mirrors about the hinge axis. With the angle of incidence $\alpha = 0$ to the DMD normal and the angle of diffraction β to the DMD normal, as shown in Fig. 2, the equation for a simple one-dimensional grating is

$$m\lambda = d \sin \beta \tag{1}$$

where d is the grating pitch, λ is the wavelength, and m is the diffraction order. From Fig. 2, $d = d_{DMD} / \sqrt{2}$, where d_{DMD} is the DMD micromirror pitch. The blaze condition for a grating under normal incidence illumination is,[11]

$$\lambda_B = \frac{d}{m} \sin 2\phi \tag{2}$$

Parameters for the so-called 0.7" XGA (1024 × 768) DMDs[**] used here are listed in Table 1. The region of efficient diffraction for a blazed grating typically extends from about 2/3 to 3/2 of λ_B, as a rule of thumb.[12] Using Eq. (2) and this rule of thumb, the blaze wavelength and the spectral range of efficient diffraction predicted by this model for each diffraction order was computed for the 0.7" XGA DMD as listed in Table 2. It is seen that the MWIR involves only the first order, while the SWIR involves orders 2-5. For all orders, the diffraction angle β_B corresponding to the blaze wavelength is $2\phi = 24°$, the same angle that is obtained from geometric ray tracing. The diffraction angles β_{B1} and β_{B2}, corresponding to wavelengths of 2/3 and 3/2 of λ_B, respectively, are as listed in Table 1, and are the same for all orders. At a given wavelength in the SWIR, where orders overlap, the diffraction angles between the different orders can be of order 10°, so the acceptance angle of the optical system after the DMD needs to be carefully designed to catch the different diffracted orders. In the VNIR, though there are even more overlapping orders, the diffraction angles are closer together so the effect on the optical design is reduced.
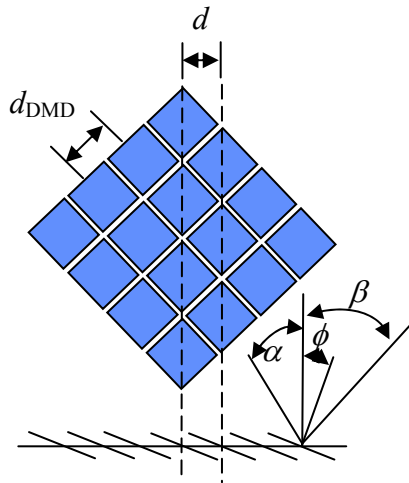

Figure 2. Description of the DMD modeled as a blazed diffraction grating. The top part of the figure depicts a section of the DMD as viewed normal to the DMD with the micromirrors in the flat state. The bottom part depicts an edge view of the same DMD section along the micromirror hinge direction (dashed lines) with all micromirrors in the on state.

Table 1. Geometrical parameters of the 0.7" XGA DMDs used in the tests performed here.

Micromirror Condition	All On
Facet Angle ϕ (degrees)	12
DMD Pitch d_{DMD} (µm)	13.68
Incidence Angle α (degrees)	0
Grating Pitch d (µm)	9.67
Lower Blaze Diffraction Angle β_{B1} (degrees)	15.73
Upper Blaze Diffraction Angle β_{B2} (degrees)	37.60

Table 2. Spectral ranges of good efficiency for each diffraction order as predicted from the blazed grating model.

Diffraction Order m	Lower Blaze Wavelength $(2/3)*\lambda_B$ (nm)	Blaze Wavelength λ_B (nm)	Upper Blaze Wavelength $(3/2)*\lambda_B$ (nm)	Spectral Range
1	2623	3934	5902	MWIR
2	1311	1967	2951	SWIR
3	874	1311	1967	NIR/SWIR
4	656	984	1475	VNIR/SWIR
5	525	787	1180	VNIR/SWIR
6	437	656	984	VNIR
7	375	562	843	VNIR
8	328	492	738	VIS
9	291	437	656	VIS
10	262	393	590	VIS
11	238	358	537	VIS
12	219	328	492	VIS
13	202	303	454	VIS

3. SWIR DMD DIFFRACTION EFFICIENCY

The diffraction efficiency of the SWIR DMD was measured using the layout depicted in Fig. 3. The collimated output of a supercontinuum fiber light source, having a continuum from 450 nm to 2500 nm, was free-space coupled over about 0.5 m into a 1.8 mm core diameter, 2 m long, fused-silica multimode fiber. The output was then collimated using a 50 mm focal length spherical lens and focused onto the SWIR DMD using a 100 mm focal length cylindrical lens (Cylindrical Lens 1 in Fig. 3). The reason for adding the multimode fiber, rather than just focusing the single-mode output of the 3 μm effective mode diameter, 2.5 W supercontinuum fiber source directly onto the DMD, was to ensure that the irradiance at the DMD stayed well below the damage threshold specification of 10 W/cm². An iris in the collimated beam was used to further reduce the light level and ensure that the beam fit within the DMD area. The line focus from the cylindrical lens was oriented parallel to the micromirror hinges, and the chief ray was at normal incidence on the DMD. The image of the source at the DMD was approximately 4 mm in the focused direction and 12 mm in the collimated direction. The irradiance of the image was not particularly uniform, since the collimated beam had a hole in the center due to intentional misalignment in the free-space coupling to prevent potentially-damaging retro-reflectance into the supercontinuum source. The diffracted light from the DMD was collected and re-collimated by another 100 mm focal length cylindrical lens (Cylindrical Lens 2 in Fig. 3), then focused using a 50 mm focal length spherical lens into the 25 mm diameter entrance aperture of a 100 mm diameter Spectralon-coated integrating sphere. The output radiance from the integrating sphere was then fiber-coupled to a VNIR/SWIR grating spectrometer for recording the radiance spectra. The DMD was mounted on a rotation stage such that it could be replaced kinematically by a gold reference mirror having a reflectance greater than 96 % across the SWIR. When the gold reference mirror was used, the rotation stage was adjusted to provide a 12° incidence angle on the mirror, thereby providing alignment of the reflected beam through the center of Cylindrical Lens 2, the spherical focusing lens, and into the sphere.
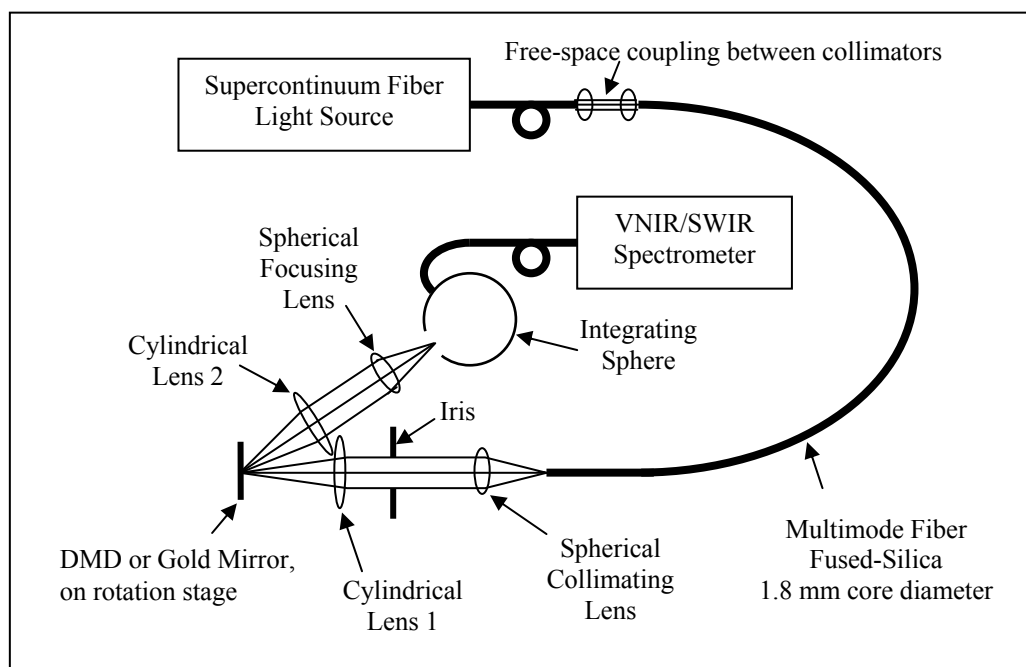

Figure 3. Layout for measurements of diffraction efficiency of the SWIR DMD using a supercontinuum fiber light source and an integrating sphere input to a VNIR/SWIR spectrometer.

A commercial Texas Instruments 0.7" XGA DMD was used as the SWIR DMD for this experiment. It was purchased with a glass window having an anti-reflection (AR) coating optimized for the SWIR spectral range. According to the specifications, this window has greater than 90 % single-pass transmission from 900 nm to beyond 2100 nm, and greater than 96 % through most of this range. This particular window coating exhibits large spectral features in the VNIR, for which it was not optimized.

The radiance spectra are shown in Fig. 4, both for the SWIR DMD with all mirrors on, and for the gold mirror. The SWIR DMD with all mirrors off provided negligible radiance when plotted on this scale, as expected. The ratio of the DMD radiance spectra to the gold mirror radiance spectra constitutes a measure of what we are calling the DMD efficiency for the purposes of this paper. These data are shown in Fig. 5. This assumes that the reflectance of the gold mirror is one. This is clearly not the case throughout the VNIR. For this reason, and considering that the DMD window is only optimized for the SWIR, the data of Fig. 5 should only be regarded as reasonably accurate (standard uncertainty is estimated at 5 %) measurements of the true DMD efficiency in the spectral range from about 900 nm to 2100 nm, as indicated on the figure. The blaze wavelengths corresponding to each diffraction order, according to the model described above, are labeled by the downward-pointing arrows in Fig. 5. Except for a slight blue shift, the experimentally-measured efficiency peaks correspond to these blaze wavelengths. The spectral ranges from Table 2, where reasonable SWIR efficiency is expected for each order, are also indicated by grey bars in Fig. 5. Within the spectral range of validity of the data, the simple diffraction model described above appears to reasonably describe the major characteristics of the efficiency data, accounting for all of the peaks. For reference, the all-mirrors-on efficiency specification in the visible range for this same DMD (with window anti-reflectance (AR) coated for the visible instead of the SWIR) is 68 %, due mainly to fill factor and reflectance of the aluminum-coated micromirrors. The data of Fig. 5 show that the effect of diffraction in the SWIR is to spectrally modulate this, but even between orders the efficiency is de-rated from the visible spec by only about 25 % at most.
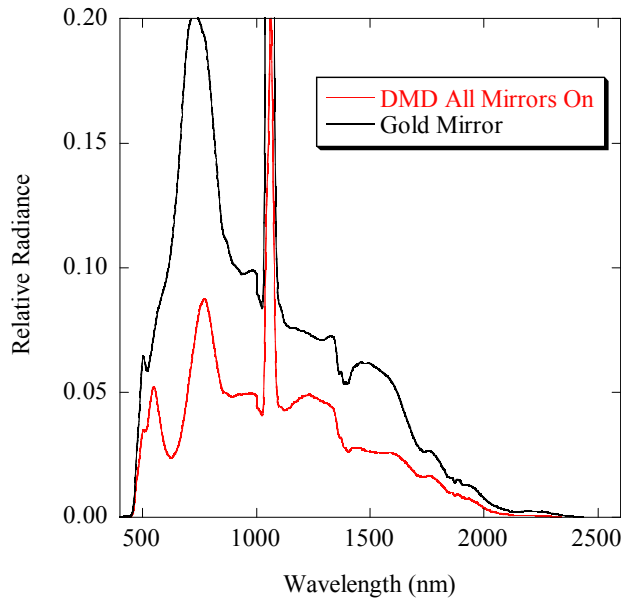

Figure 4. Radiance measurements of supercontinuum source light reflected from the SWIR DMD, and from a reference gold mirror.
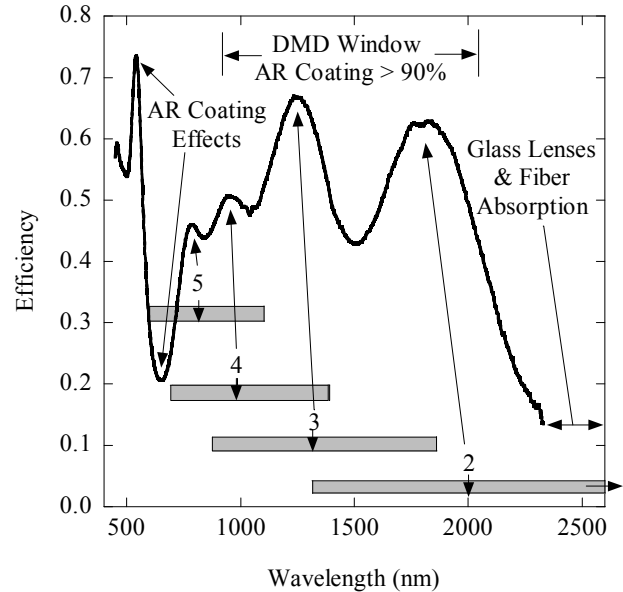
Figure 5. Efficiency measurements of the SWIR DMD computed from the data in Fig. 4 as the ratio of the DMD all-mirrors-on radiance to the reference gold mirror radiance. The peaks are near the positions of the respective grating orders from 2 through 5, which are labeled.

For application in a spectral engine as required for the HIP, it is actually the radiance spectrum, rather than the efficiency spectrum, that is of fundamental interest. Referring to the gold mirror spectra of Fig. 4, which is indicative of supercontinuum source spectrum (reduced in the range 2000 nm to 2500 nm due to the long fused silica multimode fiber and the extensive use of visible-AR coated glass optics in our setup), we note that the supercontinuum source has peaks near 1100 nm (the pump laser is at 1064 nm) and 1500 nm, precisely between the diffraction orders of the SWIR DMD. Thus the efficiency dips between orders tend to be filled in by the supercontinuum source, as shown in the DMD radiance spectra of Fig. 4, most obviously near 1500 nm. Since a spectrally-flat all-mirrors-on radiance spectra is optimal for the spectral engine of the HIP, we conclude from this preliminary study that the de-rating of the diffraction efficiency between orders in the SWIR need not necessarily degrade the HIP performance, particularly if its effects are included and compensated in the system-level design.

4. MWIR DMD DIFFRACTION EFFICIENCY

Preliminary measurements of the diffraction efficiency of the MWIR DMD in collimated mode were made using the layout depicted in Fig. 6. MWIR light from a blackbody source at a temperature of 1100 °C was collected and fed through a 1 m long chalcogenide fiber having a core diameter of 720 μm. The fiber output beam was collimated by a ZnSe lens onto the MWIR DMD. An iris was used to keep the beam diameter less than about 10 mm, so as not to illuminate the frame around the MWIR DMD. The diffracted light was directed to a MWIR spectrometer via a fold mirror. The fiber end, collimator, iris, and DMD were all mounted on a precision motorized rotation stage having its center of rotation at the DMD. Thus, the efficiency at different diffraction angles could be measured while keeping the incident beam normal to the DMD. This arrangement was enabled by the flexibility of the chalcogenide fiber, and was implemented since the blackbody source and the MWIR spectrometer were relatively large instruments that were best kept at a fixed position. The DMD was oriented such that the micromirror hinge axis was out of the page in Fig. 6, so that the diffraction angle (at least for the blazed diffraction component considered in the model) was parallel to the page, and all components were nominally in the same plane. As was done for the SWIR DMD diffraction measurements above, the MWIR DMD was kinematically replaced by a gold reference mirror, and the ratio of DMD spectrum to gold mirror spectrum constituted a measurement of the MWIR DMD efficiency.
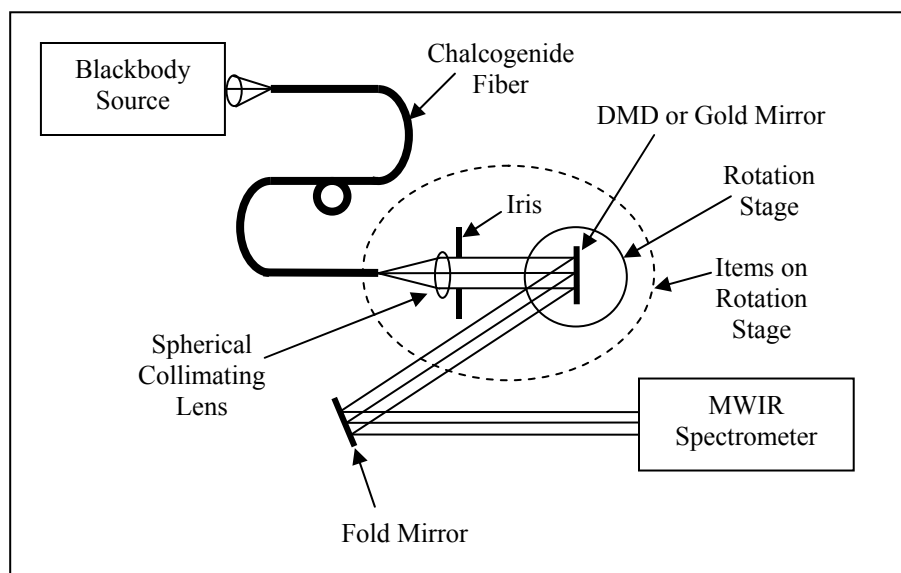

Figure 6. Experimental arrangement for measurements of diffraction efficiency of the MWIR DMD using a blackbody source and a Fourier Transform Spectrometer (FTS).

The MWIR DMD was a Texas Instruments 0.7" XGA DMD that was originally purchased with a standard glass window and aluminum coated micromirrors. This window was subsequently removed and replaced with a ZnSe window, AR coated for the 3 micrometer to 12 micrometer range, having a transmittance greater than 95 % in the MWIR. All DMD mirrors were functional after the window replacement.

While it would have been preferable to use a large-aperture integrating sphere to collect the diffracted light as was done for the SWIR DMD, this was not feasible in the MWIR since the source was not bright enough to provide practical signal-to-noise. We plan to overcome this problem in future HIP developments by the use of bright MWIR fiber-based sources.[13] For now, reasonable signal-to-noise could only be achieved by directly coupling the diffracted beam to the spectrometer as shown. Also, the MWIR spectrometer, which was a Fourier-transform spectrometer utilizing a liquid-nitrogen cooled InSb detector, had a acceptance angle of 1.3°, which was relatively narrow considering the diffracted beam divergence was of order 10° or so. Therefore, each measured spectrum captured only a narrow angular subsection of the full diffracted beam, and angular scanning was necessary to measure the full diffracted beam.

A series of spectra were collected, each with the rotation stage at a different angle, to span the full range of first order diffracted angles over the MWIR spectral range. At each angle, the signal was maximized by slight re-alignment of the tilt of the DMD and the fold mirror, to ensure optimal alignment with the spectrometer. All DMD spectra were normalized by a single gold mirror reference spectra, at an incidence (and reflected) angle of 12°. The spectral resolution was 8 cm^{-1} (corresponding to 7 nm at 3000 nm and 20 nm at 5000 nm). The efficiency spectra at each angle are shown in Fig. 7a. The envelope of these spectra can be regarded as the DMD efficiency across the full range of angles. This was determined by simply plotting the peak of each spectra versus wavelength, and is shown in Fig. 7b.

Note that this scanned angle method probably underestimates the true efficiency because of the angular sub-sampling. Evidence for this was obtained by using this method in the SWIR, with a lamp instead of a blackbody/fiber, and the SWIR DMD in place of the MWIR DMD, but with the same spectrometer. Data for both collimated incidence and focused incidence is shown in Fig. 8. The apparent efficiency dips between diffraction orders near 1100 nm and 1500 nm are much greater than those measured using the preferred method of Section 2, demonstrating the potential for error. It may therefore be that the MWIR DMD efficiency is flatter than the envelope of Fig. 7 would indicate.
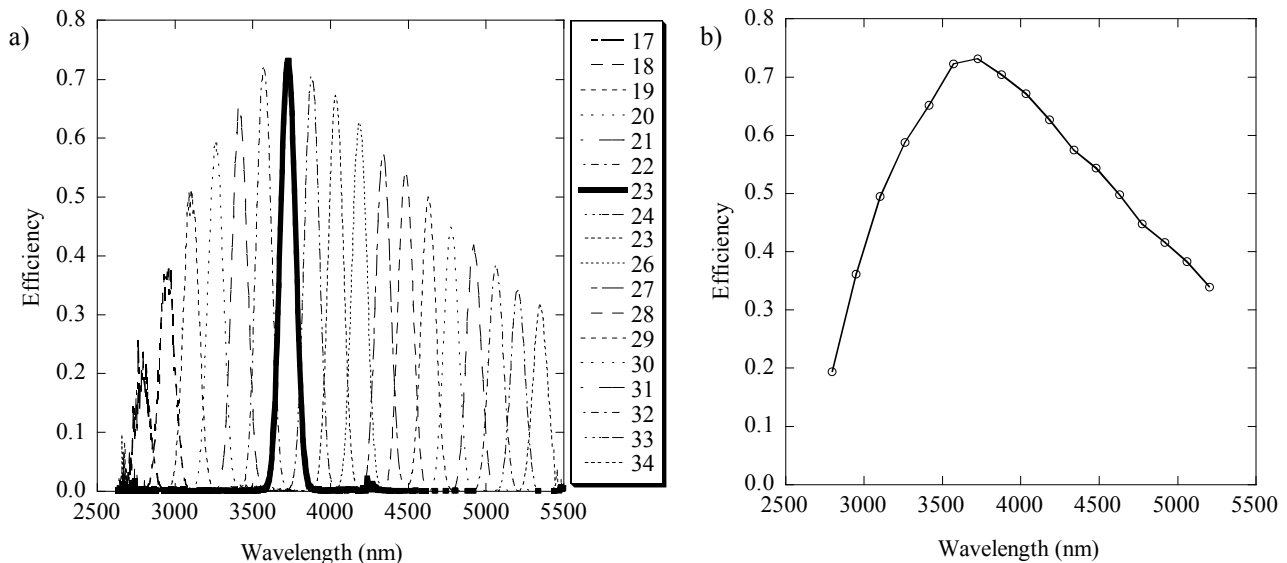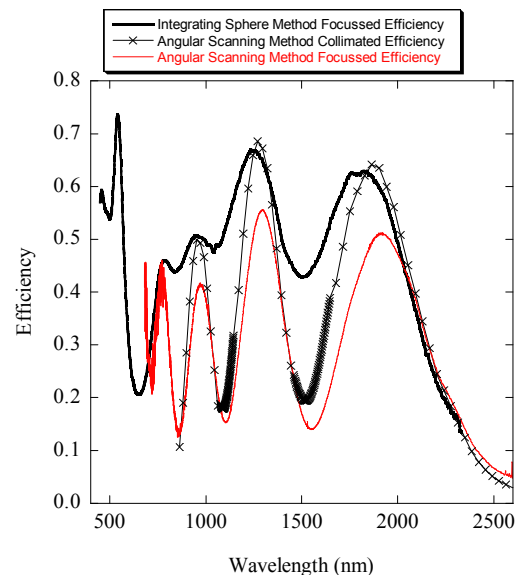

Figure 7. Measured diffraction efficiency for the MWIR DMD. a) Individual spectra taken at different diffraction angles, as indicated by the legend. The values in the legend are the diffraction angles β in degrees, with an overall absolute angular standard uncertainty of ±1°. b) Envelope of the individual spectra.

Figure 8. Measured diffraction efficiency for the same SWIR DMD using two different experimental setups, the integrating sphere method described in Section 2, and the angular scanning approach described in this section. These results show potential error sources at the edges of the diffraction orders using the angular scanning method used for the MWIR, and the differences between the curves can be regarded as an estimate of the level of uncertainty in the later method.

5. SUMMARY

We have very briefly described the HIP and its applications, referring to previously-published reports for more details. Since the applications to multispectral and hyperspectral imager testing depend strongly on projector operation in the infrared, we presented results on DMD diffraction efficiency measurements. Treating the DMD as a blazed diffraction grating, only first order diffraction contributes in the MWIR, and orders 2 through 5 contribute in the SWIR. The spectral positions of all of the observed diffraction peaks correspond reasonably well to the predictions of this blazed grating model. Also, for a large enough collection aperture, the DMD efficiency is reasonably spectrally flat and high enough for use in the HIP spectral engine, particularly with use of a supercontinuum fiber light source in the SWIR. At the blazed wavelengths the DMD efficiency in the SWIR and MWIR was near the visible specification of 68 %. Thus DMD diffraction, while it must be taken into account, is not a major problem. The DMD blazed grating diffraction model is sufficiently simple, and is reasonably confirmed experimentally, for the case of normal incidence. Thus it may provide a reliable way to incorporate the major DMD diffraction effects in design optimizations for the HIP spectral engine, and perhaps for other DMD applications in the SWIR and MWIR.

ACKNOWLEDGEMENTS

REFERENCES

[1] Rice, J. P., Brown, S. W., Neira, J. E., and Bousquet, R. R., "A hyperspectral image projector for hyperspectral imagers," *Proc. SPIE* **6565**, 65650C (2007).
[2] Brown, S. W., Myers, B., Barnes, R. A., and Rice, J. P., "Characterization of Earth observing satellite instruments for response to spectrally and spatially variable scenes," *Proc. SPIE* **6677**, 667705 (2007).
[3] Rice, J. P., Brown, S. W., and Neira, J. E., "Development of hyperspectral image projectors," *Proc. SPIE* **6297**, 629701 (2006).
[4] Brown, S. W., Rice, J. P., Neira, J. E., and Johnson, B. C., "Hyperspectral image projector for advanced sensor characterization," *Proc. SPIE* **6296**, 629602 (2006).
[5] Rice, J. P., Brown, S. W., Johnson, B. C., and Neira, J. E., "Hyperspectral image projectors for radiometric applications," *Metrologia* **43**, S61-S65 (2006).
[6] Brown, S. W., Rice, J. P., Neira, J. E., Johnson, B. C., and Jackson, J. D., "Spectrally tunable sources for advanced radiometric applications," *J. Res. Natl. Inst. Stand. Technol.* **111**, 401-410 (2006).
[7] Neira, J. E., Rice, J. P., and Amon, F. K., "Development of infrared scene projectors for testing fire-fighter cameras," *Proc. SPIE* **6942**, 694207 (2008).
[8] Brown, S. W., Rice, J. P., Allen, D. W., Zuzak, K., Livingston, E., and Litorja, M., "Dynamically programmable digital tissue phantoms," *Proc. SPIE* **6870**, 687003 (2008).
[9] Folks, W. R., López-Alonso, J. M., Monacelli, B., Weeks, A., Zummo, G., Mullally, D., and Boreman, G., "Characterization of a digital-micromirror device-based infrared scene projector," *Opt. Eng.* **44**, 086402 (2005).
[10] Duncan, W., Lee, B., Rancuret, P., Sawyers, B., Stalcup, W., Endsley, L., and Powell, D., "DLP switched blaze grating: the heart of optical signal processing," *Proc. SPIE* **4983**, 297-304 (2003).
[11] Hutley, M. H., Diffraction Gratings (Academic Press, New York, 1982), pp. 36-38.
[12] O'Shea, D. C., Elements of Modern Optical Design (Wiley, New York, 1985), pp. 327-328.
[13] Shaw, L. B., Sanghera, J. S., and Aggarwal, I. D., "IR fiber sources for scene projection," *Proc. SPIE* **6544**, 65440K (2007).